

QoS Aware Robot Trajectory Optimization with IRS-Assisted Millimeter-Wave Communications

Cristian Tatino, *Member, IEEE*, Nikolaos Pappas, *Senior Member, IEEE*, and Di Yuan, *Senior Member, IEEE*

In this paper, we consider the motion energy minimization problem for a robot that uses millimeter-wave (mm-wave) communications assisted by an intelligent reflective surface (IRS). The robot must perform tasks within given deadlines and it is subject to uplink quality of service (QoS) constraints. This problem is crucial for fully automated factories that are governed by the binomial of autonomous robots and new generations of mobile communications, i.e., 5G and 6G. In this new context, robot energy efficiency and communication reliability remain fundamental problems that couple in optimizing robot trajectory and communication QoS. More precisely, to account for the mutual dependency between robot position and communication QoS, robot trajectory and beamforming at the IRS and access point all need to be optimized. We present a solution that can decouple the two problems by exploiting mm-wave channel characteristics. Then, a closed-form solution is obtained for the beamforming optimization problem, whereas the trajectory is optimized by a novel successive-convex optimization-based algorithm that can deal with abrupt line-of-sight (LOS) to non-line-of-sight (NLOS) transitions. Specifically, the algorithm uses a radio map to avoid collisions with obstacles and poorly covered areas. We prove that the algorithm can converge to a solution satisfying the Karush-Kuhn-Tucker conditions. The simulation results show a fast convergence rate of the algorithm and a dramatic reduction of the motion energy consumption with respect to methods that aim to find maximum-rate trajectories. Moreover, we show that the use of passive IRSs represents a powerful solution to improve the radio coverage and motion energy efficiency of robots.

Index Terms—Energy efficient motion, intelligent reflective surface, millimeter-waves, robot path planning.

I. INTRODUCTION

Robotic and wireless technologies are driving the new industrial revolution, i.e., Industry 4.0, and playing a crucial role in the digital transition of manufacturing processes, warehousing, and logistics [2]. However, the massive exploitation of robots and the rising of new industrial applications, with stringent quality of service (QoS) requirements, will stress the performance of the next generation of mobile communications, i.e., 6G. Specifically, real-time industrial applications, such as augmented and virtual reality for assisted manufacturing or mining, may require Gbps for peak data rates [3], [4]. Moreover, swarms consisting of hundreds of sensing robots in the warehouses of the future may need to operate with latency and reliability requirements of 1 ms and up to 99.9999%, respectively [3], [5].

Millimeter-wave (mm-wave) spectrum has been identified as a possible solution for wireless communications in industrial scenarios [6]. However, high-band communications suffer from high blockage sensitivity [7], [8] that reduces communication reliability when a robot moves in environments with obstacles. In addition to avoiding obstacles, trajectory planning highly affects mm-wave performance as it determines whether the robot is in line-of-sight (LOS) or non-line-of-sight (NLOS). Moreover, robots are battery-limited and have tasks that are usually characterized by stringent deadlines. By optimizing the robot's movement, it is possible to dramatically decrease the robot energy consumption with a

significant reduction in the total electrical energy consumption for manufacturing processes. Consequently, in the last decades, robot trajectory planning has been one of the most relevant problem in robotics [9]–[14] and it has assumed particular importance for wirelessly connected robots, where trajectory must be optimized according to the radio coverage [15]–[17].

Beside trajectory optimization, several solutions have been proposed to enhance coverage in mm-waves scenarios, e.g., relays [18] and intelligent reflective surfaces (IRSs) [19], [20]. The latter consist of arrays of reflective elements that can be electronically controlled to adjust the angle and the phase of the reflected signals to be either added coherently or destructively for the receiver [21], [22]. Due to the short wavelength at mm-wave frequency ranges, IRSs with many reflective elements can be deployed to improve throughput and reliability of robot communications. Specifically, IRSs can provide alternative signal paths when the LOS path is blocked. Moreover, in comparison to active relays, the negligible energy consumption and the lower cost [23], [24] make passive IRSs ideal candidates for increasing the energy efficiency of fully autonomous robots. However, beamforming at the IRS must be set according to the channel that depends on the robot trajectory. Therefore, we consider a trajectory and beamforming co-optimization to minimize the motion energy consumption of a wirelessly connected robot in IRS-assisted mm-wave scenarios. To solve this problem, we propose a modified successive convex optimization (SCO) algorithm that accounts for the knowledge of the environment and a radio map to avoid collisions and satisfy time and QoS constraints.

A. Related Works

Energy-aware trajectory optimization has been one of the most crucial problems in robotics [9]–[12]. In [9], the authors model the power consumption of a DC motor-equipped robot

This work extends the preliminary study in [1] and was supported in part by CENIIT, ELLIIT, and by the European Union's Horizon 2020 research and innovation programme under the Marie Skłodowska-Curie grant agreement No. 643002 (ACT5G).

Cristian Tatino was with Department of Science and Technology (ITN), Linköping University, Sweden. He is now with Ericsson AB, 16483 Stockholm, Sweden (Email: cristian.tatino@ericsson.com). Nikolaos Pappas and Di Yuan are with Department of Science and Technology (ITN), Linköping University, Sweden (Email: nikolaos.pappas@liu.se, di.yuan@liu.se)

as a function of the speed. By optimally controlling the robot's speed, it is possible to achieve up to 50% energy-saving. The work in [10] uses a graph-based method and A* algorithm to determine the robot's minimum cost path, where the cost of an edge represents the corresponding motion energy consumption. A convex optimization approach is adopted in [11], which presents an alternating quadratic programming method to determine the path that minimizes the energy consumption in scenarios with obstacles. Multi-robot scenarios are studied in [12], where the authors propose a distributed algorithm for optimizing locations and times of robots' rendezvous. This problem includes the battery level of the robots as a constraint. The corresponding energy consumption is derived from the optimal control problem that minimizes the energy consumption along the robot trajectory. In contrast to the previously mentioned studies, the work in [15] deals with wirelessly connected robots. More precisely, the authors propose joint robot communication and motion energy minimization by controlling the transmit power and the robot's speed along a fixed trajectory.

The possibility to control the robot motion introduces a new degree of freedom for resource allocation problems in wireless communications. In the past few years, several studies have explored this topic [15]–[17], [25]–[28]. Similar to [15], the work in [16] proposes an optimal control problem for motion and communication energy minimization subject to a certain amount of data to be transmitted and power limit. In this case, multiple robots transmit data to an access point (AP) in a scenario without obstacles. In [17], the authors define a convex optimization problem to minimize the energy consumption of a moving relay and multiple mobile sensing robots by controlling trajectories and transmit power. The sensing robots move in a scenario without obstacles along paths that depend on the assigned tasks. Joint task and trajectory optimization for multiple robots is explored in [25]–[28], where [28] deals with directional communication scenarios.

Directional communications are typical for mm-wave communications and the latter has recently attracted the interest of industrial applications [4], [29]–[32]. Mm-wave connected robots are considered in [32], where the authors present several instances of an association and path planning problem in multi-AP mm-wave networks. A graph-based algorithm is used in [32] to minimize handovers and travel time of multiple robots, where a radio map is used to account for obstacles and communication blockages. However, the potentials of mm-waves transmissions for wirelessly connected robots need to be further explored. Several studies have been performed for unmanned aerial vehicle (UAV) scenarios, as shown in [33], where joint communication and trajectory planning problems are particularly relevant [34]–[39]. Specifically, similar to [32], the work in [39] uses a graph-based method and a radio map to optimize UAVs' flying distance while ensuring a target QoS requirement.

In the last few years, researchers have considered the application of IRSs to enhance UAV-user communications [40]–[42]. Specifically, in [40] and [41], authors study UAV-users communications assisted by stationary IRSs. They study joint UAV trajectory and IRS beamforming optimization problems

for maximizing the received power at the users. A similar scenario is considered in [42], where IRSs mounted on UAVs are used to establish indirect LOS links to maximize the minimum rate among user clusters. The resulting joint UAV positioning and IRS beamforming optimization problem is solved by using a hybrid particle swarm optimization-based heuristic algorithm. IRSs for enhancing low-frequency robot-AP communications are studied in [43], where the authors use a graph-based method to minimize the robot traversal time while ensuring a minimum data rate requirement at each location along the trajectory. However, as will be detailed in later sections, maximum rate trajectories and graph-based methods would provide high energy consumption or infeasible trajectories if applied to our problem.

B. Contributions

The contributions of this paper are summarized as follows:

- We consider a novel robot trajectory optimization problem with IRS-assisted mm-wave communications. The problem aims to minimize the motion energy consumption while satisfying minimum average data rate and deadline constraints. Moreover, the robot must avoid collisions with obstacles. To solve this problem, we account for the mutual dependence of the energy consumption and achieved data rate on the robot trajectory and beamforming at the IRS and AP. To the best of our knowledge, energy-efficient trajectory planning problems have not been considered for wirelessly connected robots using mm-waves, which have peculiar signal propagation conditions.
- In mm-wave scenarios, when obstacles create abrupt LOS-NLOS transitions, the received data rate is not a convex function of the robot's position. Therefore, to solve the problem mentioned above, we propose a novel SCO-based algorithm, which exploits a radio map to establish if a trajectory solution satisfies the QoS constraint. Previous SCO-based algorithms for UAVs, e.g., in [40], [41], may lead to infeasible paths or higher energy consumption if applied to our problem. Moreover, UAV communications do not present the same characteristics as wirelessly connected robots of which the altitude cannot be adapted. As in [43], graph-based methods can also include radio maps, but they may perform poorly when applied to our problem and cannot account for the average data rate constraint.
- We prove that the proposed SCO algorithm converges and, under certain conditions, it converges to a point satisfying KKT conditions. The presented method can find trajectories that avoid collisions and satisfy the QoS requirement by using radio map information. The proposed algorithm can dramatically reduce the robot's energy consumption with respect to trajectories that maximize the data rate. Finally, we show that IRSs can enhance the motion energy efficiency for QoS-constrained wirelessly connected robots. Specifically, by increasing the number of reflective elements of the IRS, the solution of the algorithm converges to the trajectory corresponding to the minimum energy consumption.

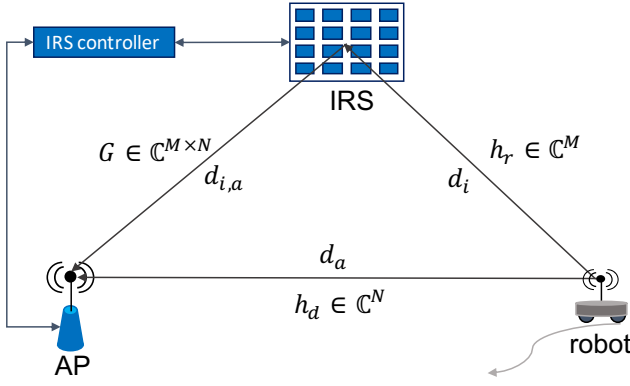


Fig. 1: A scenario consisting of an IRS-aided robot uplink communication.

The rest of the paper is organized as follows. In Section II we describe the system model. In Section III, we formulate the problem; moreover, we decouple beamforming and trajectory optimizations. In Section IV, we solve the latter by using an SCO algorithm, and in Section V, we provide performance evaluation. Finally, Section VI concludes the paper.

II. SYSTEM MODEL AND ASSUMPTIONS

We consider an industrial scenario, e.g., an industrial plant, where a robot moves from a starting position q_s to its goal q_d within a time horizon of fixed duration. The robot moves on the horizontal plane of a 3D restricted area containing several 3D obstacles. These are represented by a set \mathcal{O} of cylinders with elliptic bases and given heights.¹ The area is covered by an AP using mm-waves to which the robot needs to transmit uplink data by maintaining a given communication QoS. This is expressed as a minimum average data rate requirement² (r_{min}). The robot is equipped with a single antenna, whereas, the AP is equipped with N antennas. The robot-AP communication is assisted by an IRS consisting of a uniform linear array (ULA) of M reflective elements, of which the phase shifters are adjusted by a controller, which shares the channel state information (CSI) with the AP. A scheduler, which we assume to be co-located with the controller, optimizes the robot trajectory. The goal is to minimize the motion energy consumption accounting for both active and passive beamforming at the AP and IRS, respectively.

Notations: $(\cdot)^T$ and $(\cdot)^H$, represents the transpose and the conjugate transpose, respectively; $diag(\cdot)$ returns the diagonalization of a vector and $arg(\cdot)$ denotes the phase of a complex number. Finally, $\|\cdot\|_n$ represents the n -norm. Moreover, a summary of the notation is available in Table I.

¹Note that arbitrarily shaped obstacle can be often approximated by the intersection and the union of several convex shapes [44]. In this paper, we consider 3D cylinders with elliptic bases.

²A minimum average data rate requirement can model applications where robots can store data in a buffer and transmit when channel conditions are favorable. Moreover, this choice makes the problem more general and the solution presented in this manuscript can be easily extended to instantaneous data rate requirements.

A. Robot Motion Model

The robot must avoid collisions with obstacles and reach the destination within a given deadline. We divide the time horizon, which is defined by the deadline, in K small slots of duration Δ_t . Within a timeslot, the robot can travel for a maximum distance of $D_{max} = v_{max}\Delta_t$, where, v_{max} is the maximum speed. A trajectory of the robot is represented as a sequence of $K + 1$ positions, i.e., $\mathbf{q} = [q_0, q_1, \dots, q_K]$, where $q_0 = q_s$ and $q_K = q_d$. The terms $q_k = [x_k, y_k]$, $k = 0, \dots, K$, represent the Cartesian coordinates of the robot positions on the horizontal plane along the trajectory.

Let $q_a = [x_a, y_a]$ and $q_i = [x_i, y_i]$ represent the fixed positions of the AP and the IRS, respectively. The altitude of the robot is fixed at its antenna height z_r , whereas z_a represents the height at which the AP is installed and z_i the height of the IRS. Let v_k be the speed of the robot at the k -th timeslot. Then, the motion energy consumption of the DC motor-equipped robot along the path can be written as follows [15]:

$$E = \sum_{k=1}^{k=K} E_k = \sum_{k=1}^{k=K} c_1 v_k^2 \Delta_t + c_2 v_k \Delta_t + c_3 \Delta_t = \sum_{k=1}^K c_1 \frac{\|q_k - q_{k-1}\|_2^2}{\Delta_t} + c_2 \|q_k - q_{k-1}\|_2 + c_3 \Delta_t, \quad (1)$$

where, E_k is the energy consumption in the k -th timeslot, and c_1 , c_2 , and c_3 are positive constants depending on the characteristics of the robot and external load.

B. Channel Model

As shown in Fig. 1, let $h_r \in \mathbb{C}^M$ be the channel vector between the robot and the IRS and $G \in \mathbb{C}^{M \times N}$ denote the channel matrix between the IRS and the AP. The direct channel between the robot and the AP is represented by vector $h_d \in \mathbb{C}^N$. Then, the received baseband signal at the AP when the robot is at position q_k can be written as follows:

$$y_k = (h_{r,k}^H \Phi_k G_k + h_{d,k}^H) w_k \sqrt{p_t} s_k + \eta_k, \quad (2)$$

where, s_k and p_t are the transmit signal and the transmit power in the uplink, respectively, $\eta_k \sim \mathcal{CN}(0, \sigma^2)$ denotes the additive white Gaussian noise (AWGN). The term $w_k \in \mathbb{C}^M$ is the normalized beamforming vector at the AP, and $\Phi_k = \text{diag}(e^{j\theta_{1,k}}, \dots, e^{j\theta_{M,k}})$ is a diagonal matrix that accounts for the phase shifts $\theta_{m,k} \in [0, 2\pi]$ associated with the reflective elements of the IRS. Due to the high path loss of mm-wave transmissions, signals that are reflected more than once are subject to severe attenuations and are not considered in (2). Thus, the received signal-to-noise ratio (SNR) for q_k can be written as follows:

$$\text{SNR}_k = \frac{|(h_{r,k}^H \Phi_k G_k + h_{d,k}^H) w_k|^2}{\sigma^2} p_t, \quad (3)$$

where, the superscript H represents the hermitian. Moreover, let $d_{i,k} = \sqrt{(z_r - z_i)^2 + \|q_k - q_i\|_2^2}$, and $d_{a,k} = \sqrt{(z_r - z_a)^2 + \|q_k - q_a\|_2^2}$ be the robot-IRS and robot-AP

distances, respectively. Then, channel vectors $h_{r,k}$ and $h_{d,k}$ can be modeled as follows:

$$h_{r,k} = \sqrt{\rho d_{i,k}^{-\nu}} \tilde{h}_{r,k}, \quad (4)$$

$$h_{d,k} = \sqrt{\rho d_{a,k}^{-\mu}} \tilde{h}_{d,k}, \quad (5)$$

where, $\tilde{h}_{r,k} \sim \mathcal{CN}(0, I)$ and $\tilde{h}_{d,k} \sim \mathcal{CN}(0, I)$ are complex gaussian vectors whose elements are independent and identically distributed (i.i.d) with zero means and unit variances. The term ρ is the path loss at the reference distance of 1 m, and ν and μ are the path loss exponents of the reflected and direct channels, respectively.

Finally, for fixed Φ_k , w_k , and position q_k , we obtain the data rate by using the Shannon's formula as follows:

$$r_k = B_w \log_2(1 + SNR_k) = B_w \log_2 \left(1 + \frac{|\left(\sqrt{\rho d_{i,k}^{-\nu}} \tilde{h}_{r,k}^H \Phi_k G_k + \sqrt{\rho d_{a,k}^{-\mu}} \tilde{h}_{d,k}^H\right) w_k|^2}{\sigma^2} p_t \right). \quad (6)$$

To obtain (6) we use (3), (4), and (5) and the term B_w represents the system bandwidth. Let $\mathbf{r} = [r_0, r_1, \dots, r_K]$ be a vector, of which the elements represent the data rates along the robot trajectory $\mathbf{q} = [q_0, q_1, \dots, q_K]$. Thus, the average data rate for a trajectory \mathbf{q} is given by:

$$\bar{r} = \frac{1}{K} \sum_{k=0}^K r_k. \quad (7)$$

We can observe that \bar{r} is a function of Φ_k , w_k , and q_k . The latter is included in $d_{i,k}$, and $d_{a,k}$. Thus, the robot's position and beamforming affect the data rate, which in turn affects the trajectory due to the QoS constraint. In the next section, we formulate the joint beamforming and trajectory optimization problem introduced in this section.

III. PROBLEM FORMULATION

In this section, we formulate the problem introduced in Section II. Let $\Phi = [\Phi_0, \Phi_1, \dots, \Phi_K]$ and $\mathbf{w} = [w_0, w_1, \dots, w_K]$, then the joint robot trajectory and beamforming problem can be formulated as follows:

$$P1 : \min_{\mathbf{q}, \Phi, \mathbf{w}} E \quad (8a)$$

$$\text{s.t. } \bar{r} \geq r_{min}, \quad (8b)$$

$$\|q_k - q_{k-1}\|_2 \leq D_{max}, \quad k = 1, \dots, K, \quad (8c)$$

$$q_0 = q_s, \quad q_K = q_d, \quad (8d)$$

$$(q_k - q_{c,o})^T P_o^{-1} (q_k - q_{c,o}) \geq d_s, \quad \forall k, \forall o \in \mathcal{O}, \quad (8e)$$

$$\|w_k\|_2^2 \leq 1, \quad \forall k, \quad (8f)$$

$$\Phi_k = \text{diag}(e^{j\theta_{1k}}, \dots, e^{j\theta_{Mk}}), \quad \forall k, \quad (8g)$$

$$0 \leq \theta_{m,k} \leq 2\pi, \quad \forall m, \forall k, \quad (8h)$$

where, the objective function (8a) represents the total robot motion energy consumption along the trajectory given by (1). Note that the communication energy consumption of the robot

is negligible with respect to the motion energy consumption; hence, the objective function does not include the former. The first constraint (8b) represents the QoS requirement to complete the task, where \bar{r} is defined in (7) and r_{min} is the minimum required average data rate. Constraints (8c) allow the robot to move in a timeslot for a maximum distance of D_{max} , whereas (8d) fix the starting and the goal positions. To avoid collisions with obstacles, we include (8e). More precisely, as described in the previous section, obstacles are approximated by the intersection and the union of several ellipsoids $o \in \mathcal{O}$ on the horizontal plane. Each of them is described by a center $q_{c,o}$, and a symmetric and positive definite matrix P_o . The latter defines the length of the axis and the rotation of the ellipse. The term $d_s \geq 1$ represents a safety distance between the robot and the obstacle. Finally, constraints (8f) and (8h) impose the norm of w_k to be at most one and $\theta_{m,k}$ to be continuous, respectively.

Problem $P1$ is non-linear and non-convex. However, as we show in the following sections, it is possible to decouple the beamforming and the trajectory optimization problems. More precisely, we maximize the left-hand side (LHS) of (8b) in $P1$ by deriving closed-forms of Φ and \mathbf{w} that maximize the average data rate for each trajectory. Then, we can obtain an optimization problem equivalent to $P1$, of which the only optimization variable is \mathbf{q} . This trajectory optimization problem is solved in Section IV by using an SCO-based algorithm.

A. Average Rate Maximization

In this section, we first find closed-form solutions of Φ and \mathbf{w} that maximize average data rate \bar{r} . Specifically, for a fixed trajectory we solve the following problem:

$$P2 : \max_{\Phi, \mathbf{w}} \bar{r} \quad (9a)$$

$$\text{s.t. } (8f), (8g), (8h),$$

where, \bar{r} is given by (7).

Proposition 1. *By replacing the LHS of (8b) in $P1$, with the optimum data rate resulting from solving $P2$, we obtain a trajectory optimization problem that is equivalent to $P1$.*

Proof. We first note that in $P1$, the LHS of (8b) is the only expression that depends on Φ_k and w_k , which are not contributing to the cost (8a). Moreover, by solving $P2$, we obtain an optimum data rate expression (\bar{r}^*) that depends only on \mathbf{q} such that $\bar{r}^* \geq \bar{r} \quad \forall \mathbf{q}$. Thus, by replacing the LHS of (8b) in $P1$ with \bar{r}^* we obtain an optimization problem that depends only on \mathbf{q} with a feasible region that includes the feasible region of $P1$. \square

To solve $P2$, we can assume that the IRS and the AP are installed with a LOS link. Since in mm-wave communications the LOS path presents a much higher gain than the sum of NLOS paths, the IRS-AP channel can be approximated by a rank-one matrix [20]:

$$G_k = \sqrt{NM \rho d_{ia}^{-2}} \tilde{G}_k = \sqrt{NM} \gamma \tilde{\mathbf{a}}_k \tilde{\mathbf{b}}_k^T, \quad \forall k, \quad (10)$$

TABLE I: Summary of the notation.

\mathbf{q}	robot trajectory	q_k	k -th robot position along the trajectory
q_s	robot's starting position	q_d	robot's final position
q_a	AP's position	q_i	IRS's position
z_a	AP's height	z_i	IRS's height
$d_{a,k}$	robot-AP distance when the robot is at position q_k	$d_{i,k}$	robot-IRS distance when the robot is at position q_k
\mathcal{O}	obstacle set	$q_{c,o}$	center's position of obstacle $o \in \mathcal{O}$
K	number of timeslots	r_{min}	minimum average data rate requirement
D_{max}	maximum distance that a robot can travel in a timeslot	N	number of antennas at the AP
M	number of reflective elements at the IRS	G_k	AP-IRS channel when the robot is at position q_k
$h_{r,k}$	robot-IRS channel when the robot is at position q_k	$h_{d,k}$	robot-AP channel when the robot is at position q_k
$\theta_{m,k}$	phase shift of reflective element m when the robot is at position q_k	Φ_k	phase shifts matrix when the robot is at position q_k
w_k	normalized beamforming vector when the robot is at position q_k	B_w	system bandwidth
E	total robot motion energy consumption	E_k	robot motion energy consumption in timeslot k
SNR_k	received SNR when the robot is at position q_k	r_k	achieved data when the robot is at position q_k
\mathbf{r}	achieved data rate vector along the robot trajectory	\bar{r}	average achieved data rate
$\widehat{\text{SNR}}_k^*$	estimated optimal SNR when the robot is at position q_k	\bar{r}^*	optimized data rate
\bar{r}_{apx}^*	concave approximation of the average achieved data rate	\bar{r}_{map}	average achieved data rate obtained by the radio map
T_k	trust region for q_k	τ	trust region reduction parameter
$\hat{\nu}$	estimated robot-IRS path loss exponent	$\hat{\mu}$	estimated robot-AP path loss exponent
\mathbf{q}_0	initial solution for Algorithm 1 (RMAP)	\mathbf{q}_j	solution of Algorithm 1 (RMAP) at iteration j

where, $\gamma = \sqrt{\rho d_{ia}^{-2}}$. The term d_{ia} is the distance between the AP and the IRS that is fixed and does not depend on q_k . The path loss exponent of the LOS path between the AP and the IRS is two and ρ accounts for the path loss at the reference distance and antenna gain. The terms $\tilde{a}_k \in \mathbb{C}^M$ and $\tilde{b}_k \in \mathbb{C}^N$ are the normalized array response vectors in at q_k associated with the IRS and the AP, respectively. These can be expressed as follows:

$$\tilde{a}_k = \frac{1}{\sqrt{M}} \left[1, e^{-j\frac{2\pi}{\lambda}l\alpha_k}, \dots, e^{-j\frac{2\pi}{\lambda}l(M-1)\alpha_k} \right], \quad (11)$$

$$\tilde{b}_k = \frac{1}{\sqrt{N}} \left[1, e^{-j\frac{2\pi}{\lambda}l\beta_k}, \dots, e^{-j\frac{2\pi}{\lambda}l(N-1)\beta_k} \right], \quad (12)$$

where, α_k is the cosine of angle-of-arrival (AoA) and β_k is the cosine of angle-of-departure (AoD). The term λ is the carrier wavelength, whereas l is the antenna separation.

Maximizing P2 is equivalent to maximizing the received SNR at each robot position q_k (3). Assuming $\tilde{G}_k = \tilde{a}_k \tilde{b}_k^T$, and $\Phi_k = e^{\psi_k} \tilde{\Phi}_k$, this problem has a closed-form solution [20], which is given by:

$$\psi_k^* = -\arg \left(\left(\tilde{b}_k^T \right)^H \tilde{h}_{d,k} \right), \quad (13)$$

$$\tilde{\Phi}_k^* = \text{diag} \left(e^{-j\arg(g_{1,k})}, \dots, e^{-j\arg(g_{M,k})} \right), \quad (14)$$

$$w_k^* = \frac{\left(e^{\alpha_k} \sqrt{\rho d_{i,k}^{-\nu}} \tilde{h}_{r,k}^H \tilde{\Phi}_k^* G_k + \sqrt{\rho d_{a,k}^{-\mu}} \tilde{h}_{d,k}^H \right)^H}{\| e^{\alpha_k} \sqrt{\rho d_{i,k}^{-\nu}} \tilde{h}_{r,k}^H \tilde{\Phi}_k^* G_k + \sqrt{\rho d_{a,k}^{-\mu}} \tilde{h}_{d,k}^H \|_2}, \quad (15)$$

where, $g_k = \sqrt{\rho d_{ia}^{-2}} \left(\tilde{h}_{r,k}^* \circ \tilde{a}_k \right)$ and (\circ) denotes the element-wise product. By putting (13), (14), and (15) into (3), we obtain the following optimal SNR expression for q_k :

$$\begin{aligned} \text{SNR}_k^* &= \left(N |\rho| |\gamma|^2 \| \tilde{h}_{r,k} \|_1^2 d_{i,k}^{-\nu} + \right. \\ & 2\sqrt{N} |\rho| |\gamma| \| \tilde{h}_{r,k} \|_1 \| \tilde{b}_k^T \tilde{h}_{d,k} \| d_{i,k}^{-\nu/2} d_{a,k}^{-\mu/2} + \rho \| \tilde{h}_{d,k} \|_2^2 d_{a,k}^{-\mu} \left. \right) \frac{p_t}{\sigma^2} = \\ & \left(A d_{i,k}^{-\nu} + B d_{i,k}^{-\nu/2} d_{a,k}^{-\mu/2} + C d_{a,k}^{-\mu} \right) \frac{p_t}{\sigma^2}. \end{aligned} \quad (16)$$

In the last equality of (16), we have highlighted the dependence of SNR_k^* on the robot position q_k through the terms $d_{a,k}$ and $d_{i,k}$. However, ν and μ may rapidly change depending on the scattering environment and robot's position q_k . This can make the data rate model intractable for trajectory optimization in Section IV. For this reason, we proceed as follows: starting from (16), we assume ν and μ as constants and we estimate them, and other parameters, i.e., A , B , and C , from a set of measurements collected in a radio map. Then, in Section IV, we use the radio map information to address the dependence between the path loss exponents and the robot's position.

More precisely, given a set of channel measurements we compute (13), (14), and (15) and construct a two-dimensional (2D) radio map that provides the averaged optimal SNR_k^* for each position. Then, we can estimate $\hat{A} \geq 0$, $\hat{B} \geq 0$, $\hat{C} \geq 0$, $\hat{\nu} \geq 0$, and $\hat{\mu} \geq 0$ by fitting (16) with the radio map. This procedure results in:

$$\widehat{\text{SNR}}_k^* = \left(\hat{A} d_{i,k}^{-\hat{\nu}} + \hat{B} d_{i,k}^{-\hat{\nu}/2} d_{a,k}^{-\hat{\mu}/2} + \hat{C} d_{a,k}^{-\hat{\mu}} \right) \frac{p_t}{\sigma^2}, \quad (17)$$

where, \hat{A} , \hat{B} , \hat{C} , $\hat{\nu}$, and $\hat{\mu}$ are the estimated parameters. This model has the advantages of analytical tractability of (16) for trajectory optimization and capturing the dependence on the scattering environment.

We can use (17) in (7) to obtain an estimation of the maximum data rate resulting from the beamforming optimization:

$$\begin{aligned} \bar{r}^* &= \frac{1}{K} \sum_{k=0}^K r_k^* = \frac{B_w}{K} \sum_{k=0}^K \log_2 \left(1 + \widehat{\text{SNR}}_k^* \right) = \\ & \frac{B_w}{K} \sum_{k=0}^K \log_2 \left(1 + \left(\hat{A} d_{i,k}^{-\hat{\nu}} + \hat{B} d_{i,k}^{-\hat{\nu}/2} d_{a,k}^{-\hat{\mu}/2} + \hat{C} d_{a,k}^{-\hat{\mu}} \right) \frac{p_t}{\sigma^2} \right), \end{aligned} \quad (18)$$

where, r_k^* is the optimized data rate at position q_k . Finally, by replacing the LHS of (8b) with (18), we can decouple the beamforming and the trajectory optimization obtaining the

following problem:

$$P3 : \min_{\mathbf{q}, \Phi, \mathbf{w}} E \quad (19a)$$

$$\text{s.t. } \bar{\mathbf{r}}^* \geq \mathbf{r}_{min}, \quad (19b)$$

$$(8c), (8d), (8e),$$

where, E in (23a) is the robot energy consumption, which is given by (1).

IV. TRAJECTORY OPTIMIZATION

In this section, we provide an algorithm to solve problem $P3$ that, as introduced in Section III-A, is a trajectory optimization problem. We first derive the following:

Lemma 1: Given $c_1 \geq 0$, $c_2 \geq 0$, and $c_3 \geq 0$, the objective function of $P3$ (23a) is a convex function of \mathbf{q} .

Proof. We prove Lemma 1 by induction. As in (1), let $E|_{K=n}$ be the motion energy consumption of the robot when $K = n$: $E|_{K=n} = \sum_{k=1}^n c_1 \frac{\|q_k - q_{k-1}\|_2^2}{\Delta_t} + c_2 \|q_k - q_{k-1}\|_2 + c_3 \Delta_t$. We first prove that $E|_{K=1}$ is convex and then, by assuming that convexity holds for $E|_{K=n-1}$ we prove that $E|_{K=n}$ is a convex function of $\mathbf{q} = [q_0, \dots, q_n]$. It is easy to show that $E|_{K=1} = c_1 \frac{\|q_1 - q_0\|_2^2}{\Delta_t} + c_2 \|q_1 - q_0\|_2 + c_3 \Delta_t$ is a convex function of q_0 and q_1 because it consists of the sum of two convex functions, i.e., $c_1 \frac{\|q_1 - q_0\|_2^2}{\Delta_t}$ and $c_2 \|q_1 - q_0\|_2$, and a constant term. Now, assume that $E|_{K=n-1}$ is convex, we consider $E|_{K=n} = E|_{K=n-1} + c_1 \frac{\|q_n - q_{n-1}\|_2^2}{\Delta_t} + c_2 \|q_n - q_{n-1}\|_2 + c_3 \Delta_t$. By following the same reasoning, we can observe that $E|_{K=n}$ is the sum of three convex functions of $\mathbf{q} = [q_0, \dots, q_n]$: $E|_{K=n-1}$ that is convex by hypothesis, $\frac{\|q_n - q_{n-1}\|_2^2}{\Delta_t}$, and $c_2 \|q_n - q_{n-1}\|_2$. \square

Thus, the objective function of $P3$ is a convex function of \mathbf{q} . However, $P3$ is non-convex because the LHS of (19b) and (8e) are not concave functions of q_k . For this reason, we perform a convex local approximation of these two constraints and solve the problem iteratively by using an SCO algorithm. Starting from constraint (19b), we have the following lemma: *Lemma 2:* Given $\hat{A} \geq 0$, $\hat{B} \geq 0$, $\hat{C} \geq 0$, $\hat{\nu} \geq 0$, and $\hat{\mu} \geq 0$, $\bar{\mathbf{r}}^*$ is a convex function of $d_{a,k}$ and $d_{i,k}$ with $k = 0, \dots, K$.

Proof. See Appendix A. \square

Thus, since any convex function can be lower-bounded by its first-order Taylor expansion, we have the following:

$$\begin{aligned} \bar{\mathbf{r}}^* &\geq \bar{\mathbf{r}}_{apx}^* = \\ &\frac{\mathbf{B}_w}{K} \sum_{k=0}^K \log_2 \left(1 + \left(\hat{A} d_{i,0,k}^{-\hat{\nu}} + \hat{B} d_{i,0,k}^{-\hat{\nu}/2} d_{a,0,k}^{-\hat{\mu}/2} + \hat{C} d_{a,0,k}^{-\hat{\mu}} \right) \frac{p_t}{\sigma^2} \right) + \\ &\nabla \bar{\mathbf{r}}^* \Big|_{(d_{a,0,k}, d_{i,0,k})}^T \begin{bmatrix} d_{a,k} - d_{a,0,k} \\ d_{i,k} - d_{i,0,k} \end{bmatrix}, \end{aligned} \quad (20)$$

where, $\bar{\mathbf{r}}_{apx}^*$ is the first-order Taylor expansion of $\bar{\mathbf{r}}^*$ at expansion points $d_{a,0,k}$ and $d_{i,0,k}$. The term $\nabla \bar{\mathbf{r}}^*$ is the gradient of $\bar{\mathbf{r}}^*$ with respect to $d_{a,k}$ and $d_{i,k}$, which is given by:

$$\nabla \bar{\mathbf{r}}^* = \frac{\mathbf{B}_w}{K} \sum_{k=0}^K \begin{bmatrix} \frac{\left(-\hat{\nu} \hat{A} d_{i,k}^{-\hat{\nu}-1} - \hat{\nu}/2 \hat{B} d_{i,k}^{-\hat{\nu}/2-1} d_{a,k}^{-\hat{\mu}/2} \right) \frac{p_t}{\sigma^2}}{\ln 2 \left(1 + \left(\hat{A} d_{i,k}^{-\hat{\nu}} + \hat{B} d_{i,k}^{-\hat{\nu}/2} d_{a,k}^{-\hat{\mu}/2} + \hat{C} d_{a,k}^{-\hat{\mu}} \right) \frac{p_t}{\sigma^2} \right)} \\ \frac{\left(-\hat{\mu} \hat{C} d_{a,k}^{-\hat{\mu}-1} - \hat{\mu}/2 \hat{B} d_{i,k}^{-\hat{\nu}/2} d_{a,k}^{-\hat{\mu}/2-1} \right) \frac{p_t}{\sigma^2}}{\ln 2 \left(1 + \left(\hat{A} d_{i,k}^{-\hat{\nu}} + \hat{B} d_{i,k}^{-\hat{\nu}/2} d_{a,k}^{-\hat{\mu}/2} + \hat{C} d_{a,k}^{-\hat{\mu}} \right) \frac{p_t}{\sigma^2} \right)} \end{bmatrix}. \quad (21)$$

We now consider the following lemma:

Lemma 3: Given non-negative parameters \hat{A} , \hat{B} , \hat{C} , $\hat{\nu}$, and $\hat{\mu}$, $\bar{\mathbf{r}}_{apx}^*$ is a concave function of q_k .

Proof. See Appendix B. \square

Thus, in a small neighborhood of $d_{a,0,k}$ and $d_{i,0,k}$, we can derive $\bar{\mathbf{r}}_{apx}^*$ that is a concave function of q_k and a lower bound of $\bar{\mathbf{r}}^*$. The same reasoning can be applied to constraints (8e) leading to the following inequality:

$$\begin{aligned} (q_k - q_{c,o})^T P_o^{-1} (q_k - q_{c,o}) &\geq \\ (q_{0,k} - q_{c,o})^T P_o^{-1} (q_{0,k} - q_{c,o}) &+ \\ (q_{0,k} - q_{c,o})^T P_o^{-1} (q_k - q_{0,k}), &\end{aligned} \quad (22)$$

where, the LHS is the first-order Taylor expansion of (8e) with respect to q_k at local point $q_{0,k}$. This is an affine function of q_k .

Finally, by replacing (19b) and (8e) with (20) and (22), respectively, we can obtain a local convex approximation of $P3$ in a neighborhood of an initial feasible trajectory \mathbf{q}_0 . As shown in Algorithm 1 (*RMAP*), we can solve a sequence of local convex approximations of $P3$ that provides an upper bound to the solution of $P3$. Specifically, at each iteration j , *RMAP* solves the following problem:

$$P4 : \min_{\mathbf{q}_j} \sum_{k=1}^K c_1 \frac{\|q_{j,k} - q_{j,k-1}\|_2^2}{\Delta_t} + c_2 \|q_{j,k} - q_{j,k-1}\|_2 + c_3 \Delta_t \quad (23a)$$

$$\text{s.t. } \bar{\mathbf{r}}_{apx,j}^* \geq \mathbf{r}_{min}, \quad (23b)$$

$$\|q_{j,k} - q_{j,k-1}\|_2 \leq D_{max}, \quad \forall k, \quad (23c)$$

$$q_0 = q_s, \quad q_k = q_d, \quad (23d)$$

$$\|q_{j,k} - q_{j-1,k}\|_2 \leq T_k, \quad \forall k, \quad (23e)$$

$$\begin{aligned} (q_{j-1,k} - q_{c,o})^T P_o^{-1} (q_{j-1,k} - q_{c,o}) &+ \\ (q_{j-1,k} - q_{c,o})^T P_o^{-1} (q_{j,k} - q_{j-1,k}) &\geq 1, \quad \forall k, o, \end{aligned} \quad (23f)$$

where, $\mathbf{q}_j = [q_{j,0}, q_{j,1}, \dots, q_{j,K}]$ and $\mathbf{q}_{j-1} = [q_{j-1,0}, q_{j-1,1}, \dots, q_{j-1,K}]$ are the solutions of $P4$ at iteration j and $j-1$, respectively. More precisely, \mathbf{q}_{j-1} represents the local point at which the approximations at iteration j of constraints (19b) and (8e) are computed. These approximations are valid in a trust region of \mathbf{q}_{j-1} that is defined by constraint (23e). The trust

region size T_k may differ by position q_k . Note that the expansion points of \bar{r}^* can be obtained from $q_{j-1,k}$, as $d_{a,j-1,k} = \frac{\sqrt{(z_r - z_a)^2 + \|q_{j-1,k} - q_a\|_2^2}}{\|q_{j-1,k} - q_a\|_2}$ and $d_{i,j-1,k} = \frac{\sqrt{(z_r - z_i)^2 + \|q_{j-1,k} - q_i\|_2^2}}{\|q_{j-1,k} - q_i\|_2}$. Problem $P4$ is convex and it can be solved quickly by interior-point methods.

As introduced in Section III-A, \bar{r}^* and its approximation (\bar{r}_{apx}^*) can still diverge from the true data rate, especially when abrupt LOS-NLOS transitions occur. Thus, in $RMAP$ we introduce a solution update mechanism that differs from conventional SCO-based algorithms. The goal is to keep the feasibility of the solution at iteration j also with respect to the measured data rate obtained from the radio map and not only to its convex approximation ($\bar{r}_{apx,j}^*$). More precisely, let $\mathbf{r}_{map,j}$ be a vector of K elements, each of which consists of the measured data rate with optimized beamforming vectors at $q_{j,k}$. Let $\bar{\mathbf{r}}_{map,j}$ be the average of $\mathbf{r}_{map,j}$ along the trajectory. Then, at iteration j , $RMAP$ updates the solution, only if $\bar{\mathbf{r}}_{map,j} \geq r_{min}$, otherwise it keeps the previous solution, i.e., $\mathbf{q}_j = \mathbf{q}_{j-1}$. Furthermore, to obtain following feasible solutions, the algorithm reduces the trust-region T_k of a factor $0 \leq \tau < 1$, where k represents the position at which the measured data rate from the radio map drops the most with respect to the previous trajectory solution: $k = \underset{k}{\operatorname{argmax}} \mathbf{r}_{map,j-1,k} - \mathbf{r}_{map,j,k}$.

Algorithm 1 Radio Map Assisted Planning (RMAP)

Initial solution:

- 1: $j=0$
- 2: Find an initial feasible solution \mathbf{q}_j
- 3: Compute the motion energy consumption E_j corresponding to \mathbf{q}_j as in (23a)

SCO:

- 4: **repeat**
 - 5: $j = j + 1$
 - 6: Obtain \mathbf{q}_j and E_j by solving $P4$ with local points \mathbf{q}_{j-1}
 - 7: **if** $\bar{\mathbf{r}}_{map,j} < r_{min}$ **then**
 - 8: $\mathbf{q}_j = \mathbf{q}_{j-1}$ and $E_j = E_{j-1}$
 - 9: $T_k = \tau T_k$ with, $0 \leq \tau < 1$ and $k = \underset{k}{\operatorname{argmax}} \mathbf{r}_{map,j-1,k} - \mathbf{r}_{map,j,k}$
 - 10: **else**
 - 11: **if** $\frac{E_j - E_{j-1}}{E_{j-1}} \leq \epsilon$ **then**
 - 12: **break**
 - 13: **end if**
 - 14: **end if**
 - 15: **until** $j \geq N_{it}$
-

Hence, the algorithm maintains the feasibility with respect to both \bar{r}^* and $\bar{\mathbf{r}}_{map}$. The analytical tractability of the former is used to optimize the trajectory and understand the behavior of the data rate with respect to the distances between the robot, the AP, and the IRS. The latter ($\bar{\mathbf{r}}_{map}$) is used to capture the NLOS and LOS transitions created by the obstacles. The algorithm stops if the sequence of solutions converges or when a maximum number of iterations (N_{it}) is reached. More precisely, we can prove that the algorithm converges and, under some conditions, it converges to a Karush-Kuhn-Tucker (KKT) point of $P3$.

Theorem 1. *RMAP provides a non-increasing and convergent sequence of solutions. Moreover, if at each iteration j we have that $\bar{\mathbf{r}}_{map,j} \geq r_{min}$, RMAP converges to a KKT point of $P3$.*

Proof. The sequence of solutions provided by $RMAP$ is non increasing because, the solution of $P4$ at iteration $j-1$, \mathbf{q}_{j-1} , is a feasible solution of minimization problem $P4$ at iteration

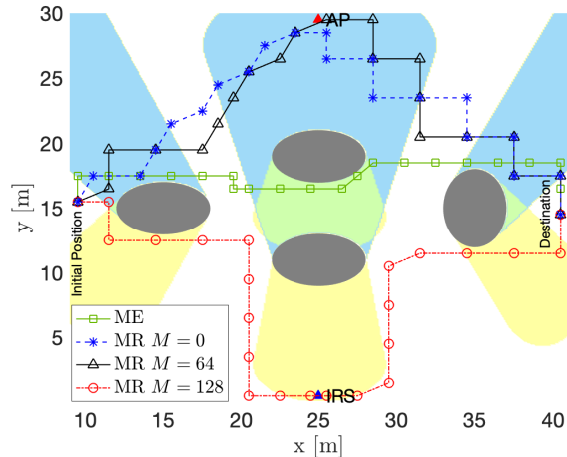


Fig. 2: Minimum energy (ME) and maximum data rate (MR) initial solutions for $K = 30$ and several values of M . Yellow, blue, and green shaded positions are in NLOS with respect to the AP, the IRS, and both, respectively. The positions in the white area are in LOS with respect to both the IRS and the AP.

j . For the rest of the proof, see Appendix C and Appendix D. \square

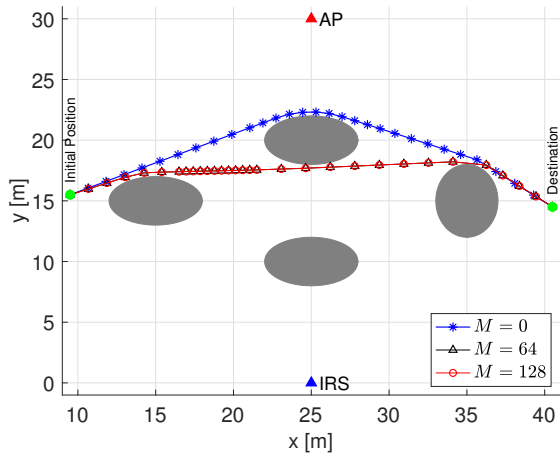
Proposition 2. *If the average measured data rate corresponding to the initial solution satisfies $\bar{\mathbf{r}}_{map,0} \geq r_{min}$, then the solution to which RMAP converges satisfies this constraint as well.*

This is a direct consequence of Lines 7-9 of $RMAP$ and Theorem 1. Namely, if $\bar{\mathbf{r}}_{map,j} < r_{min}$ then $\mathbf{q}_j = \mathbf{q}_{j-1}$. Moreover, assuming that the initial solution satisfies $\bar{\mathbf{r}}_{map,0} \geq r_{min}$ and $RMAP$ converges to a solution, this solution must satisfy the above constraint.

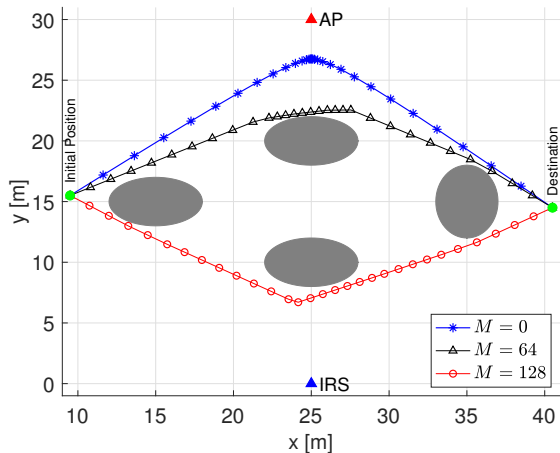
In general, the quality of a solution of SCO-based algorithms also depends on the initial solution. In this work, we obtain \mathbf{q}_0 by using a graph-based method. Specifically, we compute the shortest path on a time-expanded graph as done in [32]. The edges and vertices of the graph are defined on a discrete set of positions that are free from obstacles. In each timeslot, a robot may either stay at a vertex or move to an adjacent one. The distance between vertices is set according to the robot's maximum speed. On this graph, the costs of the edges are set to generate two different initial solutions. The first one minimizes the motion energy consumption (ME), whereas the second solution maximizes the data rate (MR). The radio map is used to obtain the SNR and the data rate for the positions corresponding to vertices and edges. Then, $RMAP$ uses the minimum energy initial solution if it is feasible and the maximum data rate initial solution, otherwise. If the latter is not feasible, the algorithm declares infeasibility.

V. NUMERICAL RESULTS

In this section, we provide a numerical validation of $RMAP$ for solving $P3$. For our simulations, we consider a 50×30 m² rectangular-shaped indoor scenario. The robot's starting position is [9.5, 14.5], whereas the destination is [40.5, 14.5]. There are an AP and an IRS placed at [25, 30] and [25, 0],



(a) $r_{min} = 2.0$ Gbps.

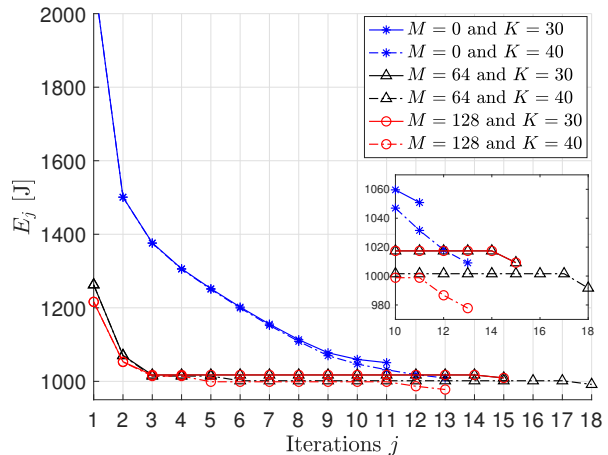


(b) $r_{min} = 2.5$ Gbps.

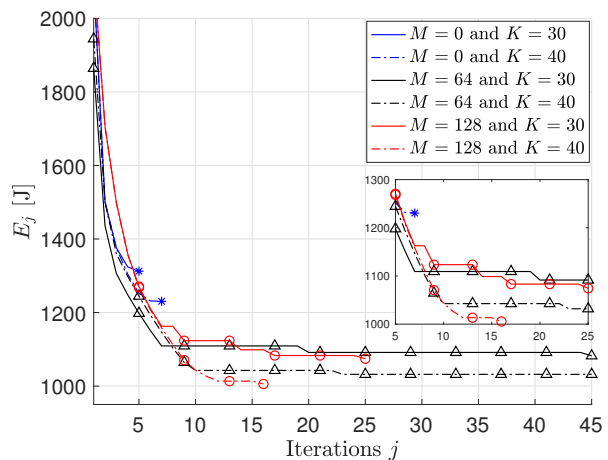
Fig. 3: Robot trajectories to which $RMAP$ converges for $K = 30$, and several values of M and r_{min} .

respectively, operating in the 60 GHz band as in [31], with bandwidth $B_w = 200$ MHz. The height of the AP is 5 m, whereas we set the heights of the IRS and the robot's antenna to 2.5 m and 0.5 m, respectively. For sake of clarity, we first present results for a scenario consisting of four ellipse obstacles that are placed as in Fig. 2, represented by grey shaded areas (*base scenario*). This scenario includes several robot-AP and robot-IRS channel conditions, i.e., LOS and NLOS positions. Then, we present results that are averaged over ten instances in which 20 obstacles are randomly placed (*random scenario*). In both scenarios, the length, width, and height of obstacles are 6 m, 4 m, and 2 m, respectively.

Similar to [31], the path loss at a reference distance of 1 m is 68 dB, and the path loss exponent of the robot-AP and robot-IRS channels are set to 2 for LOS, and 4.5 for NLOS. Without loss of generality the antenna gain of the reflective elements are set to 0 dBi. Moreover, we set the transmit and the noise powers to 20 dBm, and -80 dBm, respectively. We show the results, for several values of M and r_{min} , and, unless otherwise specified, we set the following parameters values: $K = 30$, $\tau = 0.5$, $N = 16$, $\Delta_t = 1$ s, $v_{max} = 3$ m/s, $d_s =$



(a) $r_{min} = 2.0$ Gbps.



(b) $r_{min} = 2.5$ Gbps.

Fig. 4: Energy consumption corresponding to the sequence of solutions \mathbf{q}_j provided by $RMAP$ for several values of M , r_{min} , and K .

1.35, $N_{it} = 100$, $\epsilon = 0.01$, $T = 1$ m, $c_1 = 4.39$, $c_2 = 24.67$, and $c_3 = 14.77$ [15]. Finally, to derive (17), we estimate $\hat{A} \geq 0$, $\hat{B} \geq 0$, $\hat{C} \geq 0$, $\hat{v} \geq 0$, and $\hat{\mu} \geq 0$. These parameters are obtained by fitting (16) on a radio map by solving a non-linear least squares problem. The radio map is obtained from the average of 10.000 channel measurements on a grid of 500×300 points.

A. Base Scenario

In Fig. 2, we first show ME and MR initial solutions for several values of M . Note that the MR initial solution considers the trajectory that maximizes the data rate. Such a trajectory tends to avoid NLOS areas with respect to either the AP or to the IRS depending on the number of reflective elements (M) of the latter.

In Fig. 3a we show robot trajectories resulting from $RMAP$ for $K = 30$, $r_{min} = 2.0$ Gbps, and several values of M . For $M = 0$, we can observe that the robot avoids NLOS areas with respect to the AP. Specifically, $RMAP$ uses initial solution MR. When M increases, the IRS enhances the coverage

such that the robot can find a trajectory with lower energy consumption (E) by using initial solution ME. The resulting trajectory crosses the NLOS area with respect to both the AP and the IRS. Note that, for $r_{min} = 2.0$ Gbps, values of M that are higher than 64 do not provide further gain, thus the trajectories for $M = 64$ and $M = 128$ coincide. This is not true when $r_{min} = 2.5$ Gbps, for which the trajectories are shown in Fig. 3b. More precisely, when r_{min} increases, $RMAP$ selects the MR initial solutions for all the values of M and the resulting paths are either closer to the AP or the IRS to improve the coverage and increase the data rate. For $M = 0$ and $M = 64$ the robot trajectories avoid completely NLOS areas with respect to the AP, whereas, for $M = 128$, the paths that are closer to the IRS provide higher data rates. We can also observe that the robot decreases the speed when the data rate is higher. Specifically, in LOS positions that are closer to the AP and the IRS, the robot travels for a smaller distance in each timeslot to exploit better coverage.

In general, E increases for higher values of r_{min} and decreases when M and K increase. This is more prominent in Fig. 4a and Fig. 4b where we show energy consumption E_j corresponding to the sequence of solutions q_j provided by $RMAP$ for $r_{min} = 2.0$ Gbps and $r_{min} = 2.5$ Gbps, respectively. First, we can observe that, by increasing M , $RMAP$ converges to paths with lower E . The energy consumption also decreases when K increases. Specifically, for a fixed value of Δ_t , higher values of K correspond to longer deadlines and the robot can decrease the speed to reach the destination. Then, as described by (1), lower speeds correspond to lower values of E . Moreover, we can observe that E_j is non-increasing and $RMAP$ converges in few iterations. However, as explained and shown better in the following section, the number of iterations within which $RMAP$ converges depends on the value of τ .

B. Random Scenario

In this section, we present results that are averaged over 10 instances in which $N_o = 20$ obstacles are randomly placed. The area, the obstacles dimension, and the robot's starting position and destination are the same that are used for Section V-A. In Fig. 5, we show the average energy consumption corresponding to the trajectory resulting from $RMAP$ for several values of M , K , and r_{min} . Moreover, we show the average E corresponding to robot trajectories that maximize the data rate under time and collision avoidance constraints. In addition, Fig. 5 depicts lower bounds to the average energy consumption that are computed by solving a relaxed version of problem $P3$, where obstacle avoidance (8e) and QoS (19b) constraints are relaxed. This relaxation results in a convex optimization problem that provides lower bounds to solutions of $P3$. Conversely, it is important to highlight that $RMAP$ provides upper bounds to $P3$.

Maximum data rate trajectories are obtained by solving a modified version of $P3$, where the LHS of (19b) represents the objective function of the problem. This problem is solved by using an SCO-based algorithm where, as done in Section IV for $P3$, the objective function and the LHS of (8e) are approximated by convex functions. Note that maximum-rate

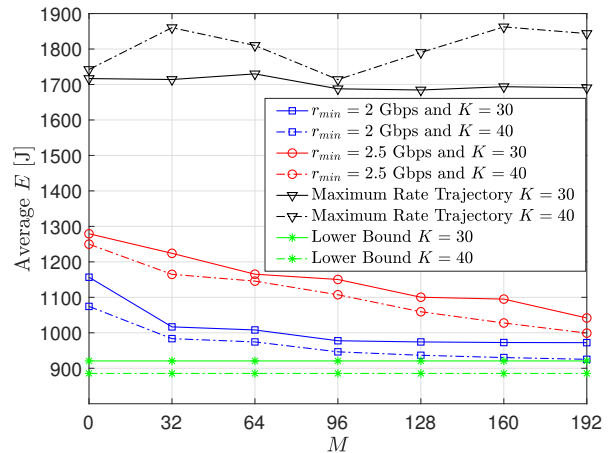


Fig. 5: Average E corresponding to solutions of $RMAP$ and maximum data rate trajectories for several values of M , r_{min} , and K . Moreover, we show lower bounds to average E for various values of K .

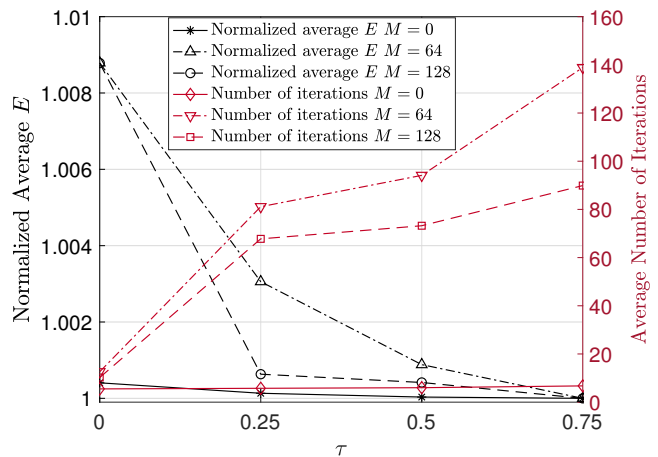


Fig. 6: Normalized average E (black) and number of iterations (red) within which $RMAP$ converges for several values of M , τ , $K = 30$, and $r_{min} = 2.5$ Gbps.

trajectories are feasible solutions of $P3$, whereas trajectories resulting from computing the lower bounds may be not.

In Fig. 5, we can observe that, for both $r_{min} = 2.0$ Gbps and $r_{min} = 2.5$ Gbps, $RMAP$ can reduce dramatically the average E with respect to the maximum data rate approach. The gain is close to 100% for $r_{min} = 2.0$ Gbps and $K = 40$. Moreover, Fig. 5 shows that the average E resulted from $RMAP$ decreases and approaches the lower bound as M increases. Specifically, by increasing the number of reflective elements at the IRS we enhance the coverage, and the robot can find a higher number of feasible trajectories. However, while for $r_{min} = 2.5$ Gbps, increasing M results in a monotonic decrease of E , for $r_{min} = 2.0$ Gbps, we note that above a certain threshold ($M \geq 32$) increasing the value of M does not provide significant gains. Additional gain can be obtained by increasing the values of K as also explained in Section V-A. These observations do not hold for maximum data rate trajectories for which the solutions have not monotonic decreasing behaviors with respect to M .

Finally, in Fig. 6 we show the effects of parameter τ

on the number of iterations within which *RMAP* converges. Moreover, we show the average E corresponding to the solutions within which *RMAP* converges for several values of τ . These are normalized to the solutions that are obtained for $\tau = 0.75$. As explained in Section IV, in each iteration of *RMAP* for which the solution does not satisfy $\bar{r}_{map,j} \geq r_{min}$, we multiply the trust region size (of the position where the data rate drops the most) by τ . Specifically, when τ is smaller, the sizes of the trust regions may decrease faster leading to a faster algorithm convergence. This can be observed in Fig. 6, which shows the tradeoff between the number of iterations that *RMAP* needs to converge and the quality of the solution. The latter improves when τ grows, which leads to lower values of average E . However, when $\tau = 0$, *RMAP* provides solutions in fewer iterations and negligible loss ($\leq 1\%$) with respect to the ones provided for $\tau = 0.75$.

VI. CONCLUSION

In this work, we have proposed a novel robot trajectory optimization problem with QoS constrained communications for minimizing the motion energy consumption. The robot must avoid collisions with obstacles, reach the destination within a deadline, and transmit data to an AP operating at mm-wave frequency bands and assisted by an IRS. The uplink transmission is subject to a minimum average data rate. To the best of our knowledge, energy-efficient trajectory planning problems for wirelessly connected robots have not been considered for mm-wave communications. We have proposed a solution that accounts for the challenging signal propagation conditions at such high frequencies and the mutual dependence between the channel conditions and the robot trajectory. Specifically, we have decoupled the beamforming and the trajectory optimization problems by exploiting the mm-wave propagation characteristics. The latter is solved by an SCO-based algorithm (*RMAP*) for which the convergence is proved. *RMAP* can deal with sudden data rate drops due to LOS-NLOS transitions by using the information that is stored in a radio map. Given this information, *RMAP* can find trajectories that avoid obstacles and poorly connected areas for satisfying data rate requirements.

We have shown trajectories and corresponding energy consumptions at which the algorithm converges for several scenarios and system parameters. The algorithm converges in few iterations to solutions that approach the lower bound to the energy consumption, which is dramatically reduced with respect to trajectories that maximize the data rate. Finally, we have shown that, by increasing the number of IRS's reflective elements, we can improve the coverage and reduce the energy consumption of wirelessly connected robots. Thus, given the negligible power consumption of passive IRSs, they represent powerful solutions to enhance the energy efficiency of fully connected and autonomous factories.

APPENDIX A

To prove Lemma 2, we prove that \mathbf{r}_k^* , which is the estimated data rate at position q_k , is a convex function of $d_{i,k}$ and $d_{a,k}$. Then, $\bar{\mathbf{r}}^*$ is convex because it is a sum of convex functions.

We first compute the partial derivatives of \mathbf{r}_k^* with respect to $d_{i,k}$ and $d_{a,k}$. These are given by:

$$\frac{\partial \mathbf{r}_k^*}{\partial d_{i,k}} = \frac{\left(-\hat{\nu} \hat{A} d_{i,k}^{-\hat{\nu}-1} - \hat{\nu}/2 \hat{B} d_{i,k}^{-\hat{\nu}/2-1} d_{a,k}^{-\hat{\mu}/2}\right) \frac{p_t}{\sigma^2}}{F_k}, \quad (24)$$

$$\frac{\partial \mathbf{r}_k^*}{\partial d_{a,k}} = \frac{\left(-\hat{\mu} \hat{C} d_{a,k}^{-\hat{\mu}-1} - \hat{\mu}/2 \hat{B} d_{i,k}^{-\hat{\nu}/2} d_{a,k}^{-\hat{\mu}/2-1}\right) \frac{p_t}{\sigma^2}}{F_k}, \quad (25)$$

where, $F_k = \ln(2) \left(1 + \left(\hat{A} d_{i,k}^{-\hat{\nu}} + \hat{B} d_{i,k}^{-\hat{\nu}/2} d_{a,k}^{-\hat{\mu}/2} + \hat{C} d_{a,k}^{-\hat{\mu}}\right) \frac{p_t}{\sigma^2}\right) > 0$. Then, the second order partial derivatives are given by:

$$\frac{\partial^2 \mathbf{r}_k^*}{\partial d_{i,k}^2} = \frac{\left(\hat{\nu}(\hat{\nu}+1) \hat{A} d_{i,k}^{-\hat{\nu}-2} + \hat{\nu}/2(\hat{\nu}+1) \hat{B} d_{i,k}^{-\hat{\nu}/2-2} d_{a,k}^{-\hat{\mu}/2}\right) F_k \frac{p_t}{\sigma^2}}{F_k^2} - \frac{\ln(2) \left(-\hat{\nu} \hat{A} d_{i,k}^{-\hat{\nu}-1} - \hat{\nu}/2 \hat{B} d_{i,k}^{-\hat{\nu}/2-1} d_{a,k}^{-\hat{\mu}/2}\right)^2 \frac{p_t^2}{\sigma^4}}{F_k^2}, \quad (26)$$

$$\frac{\partial^2 \mathbf{r}_k^*}{\partial d_{a,k}^2} = \frac{\left(\hat{\mu}(\hat{\mu}+1) \hat{C} d_{a,k}^{-\hat{\mu}-2} + \hat{\mu}/2(\hat{\mu}+1) \hat{B} d_{i,k}^{-\hat{\nu}/2} d_{a,k}^{-\hat{\mu}/2-2}\right) F_k \frac{p_t}{\sigma^2}}{F_k^2} - \frac{\ln(2) \left(-\hat{\mu} \hat{C} d_{a,k}^{-\hat{\mu}-1} - \hat{\mu}/2 \hat{B} d_{i,k}^{-\hat{\nu}/2} d_{a,k}^{-\hat{\mu}/2-1}\right)^2 \frac{p_t^2}{\sigma^4}}{F_k^2}, \quad (27)$$

$$\frac{\partial^2 \mathbf{r}_k^*}{\partial d_{i,k} \partial d_{a,k}} = \frac{\left((\hat{\mu}/2)(\hat{\nu}/2) \hat{B} d_{i,k}^{-\hat{\nu}/2-1} d_{a,k}^{-\hat{\mu}/2-1}\right) F_k \frac{p_t}{\sigma^2}}{F_k^2} - \frac{\ln(2) \left(-\hat{\nu} \hat{A} d_{i,k}^{-\hat{\nu}-1} - \hat{\nu}/2 \hat{B} d_{i,k}^{-\hat{\nu}/2-1} d_{a,k}^{-\hat{\mu}/2}\right) \frac{p_t^2}{\sigma^4}}{F_k^2} \times \frac{\left(-\hat{\mu} \hat{C} d_{a,k}^{-\hat{\mu}-1} - \hat{\mu}/2 \hat{B} d_{i,k}^{-\hat{\nu}/2} d_{a,k}^{-\hat{\mu}/2-1}\right) \frac{p_t^2}{\sigma^4}}{F_k^2}. \quad (28)$$

We observe that $\frac{\partial^2 \mathbf{r}_k^*}{\partial d_{i,k}^2} > 0$, $\frac{\partial^2 \mathbf{r}_k^*}{\partial d_{a,k}^2} > 0$ and $\frac{\partial^2 \mathbf{r}_k^*}{\partial d_{i,k}^2} \frac{\partial^2 \mathbf{r}_k^*}{\partial d_{a,k}^2} - \left(\frac{\partial^2 \mathbf{r}_k^*}{\partial d_{i,k} \partial d_{a,k}}\right)^2 > 0$. Therefore, the Hessian is positive definite and \mathbf{r}_k^* is a convex function of $d_{i,k}$ and $d_{a,k}$.

APPENDIX B

We prove Lemma 3 by following the same reasoning of Appendix A. Note that $\bar{\mathbf{r}}_{apx}^*$ in (20) is the sum of $K+1$ functions

each of them depending only on the robot's position q_k :

$$\begin{aligned} \bar{r}_{app}^* &= \frac{1}{K} \sum_{k=0}^K r_{app,k}^* = \\ & \frac{1}{K} \sum_{k=0}^K B_w \log_2 \left(1 + \left(\widehat{A} d_{i,0,k}^{-\widehat{\nu}} + \widehat{B} d_{i,0,k}^{-\widehat{\nu}/2} d_{a,0,k}^{-\widehat{\mu}/2} + \widehat{C} d_{a,0,k}^{-\widehat{\mu}} \right) \frac{p_t}{\sigma^2} \right) \\ & - \frac{\partial r_k^*}{\partial d_{a,k}} \Big|_{(d_{a,0,k}, d_{i,0,k})} d_{a,0,k} - \frac{\partial r_k^*}{\partial d_{i,k}} \Big|_{(d_{a,0,k}, d_{i,0,k})} d_{i,0,k} \\ & + \frac{\partial r_k^*}{\partial d_{a,k}} \Big|_{(d_{a,0,k}, d_{i,0,k})} \sqrt{(z_r - z_a)^2 + (x_k - x_a)^2 + (y_k - y_a)^2} \\ & + \frac{\partial r_k^*}{\partial d_{i,k}} \Big|_{(d_{a,0,k}, d_{i,0,k})} \sqrt{(z_r - z_i)^2 + (x_k - x_i)^2 + (y_k - y_i)^2}, \end{aligned} \quad (29)$$

where, $\frac{\partial r_k^*}{\partial d_{i,k}} < 0$ and $\frac{\partial r_k^*}{\partial d_{a,k}} < 0$ are given by (24) and (25), respectively. Note that in (29) we have replaced q_k with $[x_k, y_k]$. Let us define $D_k = \sqrt{(z_r - z_a)^2 + (x_k - x_a)^2 + (y_k - y_a)^2}$, then, we can compute the partial derivatives of $r_{app,k}^*$ with respect to x_k and y_k as follows:

$$\begin{aligned} \frac{\partial r_{app,k}^*}{\partial x_k} &= \frac{\partial r_k^*}{\partial d_{a,k}} \Big|_{(d_{a,0,k}, d_{i,0,k})} \frac{(x_k - x_a)}{D_k} + \\ & \frac{\partial r_k^*}{\partial d_{i,k}} \Big|_{(d_{a,0,k}, d_{i,0,k})} \frac{(x_k - x_i)}{D_k}, \end{aligned} \quad (30)$$

$$\begin{aligned} \frac{\partial r_{app,k}^*}{\partial y_k} &= \frac{\partial r_k^*}{\partial d_{a,k}} \Big|_{(d_{a,0,k}, d_{i,0,k})} \frac{(y_k - y_a)}{D_k} + \\ & \frac{\partial r_k^*}{\partial d_{i,k}} \Big|_{(d_{a,0,k}, d_{i,0,k})} \frac{(y_k - y_i)}{D_k}, \end{aligned} \quad (31)$$

The second order partial derivatives are given by:

$$\begin{aligned} \frac{\partial^2 r_{app,k}^*}{\partial x_k^2} &= \frac{\partial r_k^*}{\partial d_{a,k}} \Big|_{(d_{a,0,k}, d_{i,0,k})} \frac{(y_k - y_a)^2 + (z_k - z_a)^2}{D_k^3} + \\ & \frac{\partial r_k^*}{\partial d_{i,k}} \Big|_{(d_{a,0,k}, d_{i,0,k})} \frac{(y_k - y_i)^2 + (z_k - z_i)^2}{D_k^3}, \end{aligned} \quad (32)$$

$$\begin{aligned} \frac{\partial^2 r_{app,k}^*}{\partial y_k^2} &= \frac{\partial r_k^*}{\partial d_{a,k}} \Big|_{(d_{a,0,k}, d_{i,0,k})} \frac{(x_k - x_a)^2 + (z_k - z_a)^2}{D_k^3} + \\ & \frac{\partial r_k^*}{\partial d_{i,k}} \Big|_{(d_{a,0,k}, d_{i,0,k})} \frac{(x_k - x_i)^2 + (z_k - z_i)^2}{D_k^3}, \end{aligned} \quad (33)$$

$$\begin{aligned} \frac{\partial^2 r_{app,k}^*}{\partial x_k \partial y_k} &= \frac{\partial r_k^*}{\partial d_{a,k}} \Big|_{(d_{a,0,k}, d_{i,0,k})} \frac{(x_k - x_a)(y_k - y_a)}{D_k^3} + \\ & \frac{\partial r_k^*}{\partial d_{i,k}} \Big|_{(d_{a,0,k}, d_{i,0,k})} \frac{(x_k - x_i)(y_k - y_i)}{D_k^3}, \end{aligned} \quad (34)$$

Note that $\frac{\partial^2 r_{app,k}^*}{\partial x_k^2} < 0$ and $\frac{\partial^2 r_{app,k}^*}{\partial y_k^2} < 0$ because $\frac{\partial r_k^*}{\partial d_{i,k}} \Big|_{(d_{a,0,k}, d_{i,0,k})} < 0$ and $\frac{\partial r_k^*}{\partial d_{a,k}} \Big|_{(d_{a,0,k}, d_{i,0,k})} < 0$ are negative terms $\forall d_{a,0,k} > 0, \forall d_{i,0,k} > 0$. Furthermore, we have that $\frac{\partial^2 r_{app,k}^*}{\partial x_k^2} \frac{\partial^2 r_{app,k}^*}{\partial y_k^2} - \left(\frac{\partial^2 r_{app,k}^*}{\partial x_k \partial y_k} \right)^2 > 0$. Therefore, by following the leading principal minors criteria, the Hessian is negative definite and $r_{app,k}^*$ is a concave function of $q_k = [x_k, y_k]$.

APPENDIX C

In this appendix, we prove that the sequence of solutions provided by *RMAP* converges to a KKT point of *P3* if, in each iteration j , $\bar{r}_{map,j} \geq r_{min}$. We first observe that, when this condition holds, Lines 7-9 of *RMAP* does not affect the solution. Then, solving *P3* by *RMAP*, is equivalent to solving *P3* by using an SCO algorithm for which the convergence to a KKT point of *P3* follows from [45]. The convergence is guaranteed for every feasible initial solution and every trust region size $T_k > 0$. This proves the second part of Theorem 1.

APPENDIX D

Now, we prove that *RMAP* converges even when condition $\bar{r}_{map,j} \geq r_{min}$ does not hold for each iteration. More precisely, for each iteration n such that $\bar{r}_{map,n} < r_{min}$, *RMAP* sets $\mathbf{q}_n = \mathbf{q}_{n-1}$ and decreases T_k for a certain position q_k . Then, we can have one of the following three cases:

- *Case 1*: $T_k > 0, \forall k$. *RMAP* continues solving problem *P3* from iteration $j = n + 1$ with \mathbf{q}_{n-1} as the initial feasible solution and $T_k > 0, \forall k$. As proved in Appendix C, if for the successive iterations, i.e., $\forall j > n + 1$, we have that $\bar{r}_{map,j} \geq r_{min}$, *RMAP* still converges to a KKT point of *P3*. Otherwise, for each iteration n such that $\bar{r}_{map,n} < r_{min}$, Lines 8 and 9 are repeated and this proof follows either *Case 1* or *Case 2* whether $T_k > 0, \forall k$ or $T_k = 0$ for a certain position, respectively. If $T_k = 0, \forall k$, the proof follows *Case 3*.
- *Case 2*: $T_k = 0$ for a certain position q_k and iteration n . In this case, we have that constraint (23e) of *P4* becomes:

$$\|q_{j,k} - q_{j-1,k}\|_2 \leq T_k = 0, \forall j > n.$$

This is equivalent to adding the following affine constraints to *P3* and *P4*, respectively:

$$q_k = q_{n-1,k} \text{ and } q_{j,k} = q_{n-1,k}, \forall j > n.$$

The constraints, in fact, fix the position of the robot q_k . Given these constraints, we are free to set $T_k > 0$. Thus, from iteration $j > n$, *RMAP* solves a modified version of *P3* (*P3'*), starting from initial solution q_{n-1} and $T_k > 0, \forall k$ by iteratively solving a modified version of *P4* (*P4'*). Note that adding this affine constraint to *P3* and *P4* does not change the convexity of the latter. As done in Appendix C, we can prove that *RMAP* converges to a KKT point of *P3'* if $\forall j > n + 1$, we have that $\bar{r}_{map,j} \geq r_{min}$ holds. Otherwise, if $\bar{r}_{map,j} < r_{min}$ for a certain iteration, the proof follows *Case 1* or *Case 2*, whether $T_k > 0, \forall k$ or $T_k = 0$ for a certain position, respectively. If $T_k = 0, \forall k$, the proof follows *Case 3*.

- *Case 3*: $T_k = 0, \forall k$. In this case, the robot's position for each $k = 0, \dots, K$ is fixed, and *RMAP* has converged to a solution.

Thus, we have that *RMAP* either converges to a KKT point of *P3* or to a KKT point of a modified problem where, for some or for all $k = 0, \dots, K$, the robot's positions are fixed.

REFERENCES

- [1] C. Tatino, N. Pappas, and D. Yuan, "Robot trajectory planning with QoS constrained IRS-assisted millimeter-wave communications," in *IEEE International Conference on Communications (ICC)*, 2021.
- [2] R. Sabella, A. Thuelig, M. C. Carrozza, and M. Ippolito, "Industrial automation enabled by robotics, machine intelligence and 5G," *Ericsson Technology Review*, 2018.
- [3] M. Giordani, M. Polese, M. Mezzavilla, S. Rangan, and M. Zorzi, "Toward 6G networks: Use cases and technologies," *IEEE Communications Magazine*, vol. 58, no. 3, pp. 55–61, 2020.
- [4] M. Cheffena, "Industrial wireless communications over the millimeter wave spectrum: opportunities and challenges," *IEEE Communications Magazine*, vol. 54, no. 9, pp. 66–72, Sep. 2016.
- [5] J. Wen, L. He, and F. Zhu, "Swarm robotics control and communications: Imminent challenges for next generation smart logistics," *IEEE Communications Magazine*, vol. 56, no. 7, pp. 102–107, 2018.
- [6] M. Norin et al., "5G spectrum for local industrial networks," *Ericsson White Paper*, 2021.
- [7] I. K. Jain, R. Kumar, and S. S. Panwar, "The impact of mobile blockers on millimeter wave cellular systems," *IEEE Journal on Selected Areas in Communications*, vol. 37, no. 4, pp. 854–868, 2019.
- [8] C. Tatino, I. Malanchini, D. Aziz, and D. Yuan, "Beam based stochastic model of the coverage probability in 5G millimeter wave systems," in *15th International Symposium on Modeling and Optimization in Mobile, Ad Hoc, and Wireless Networks (WiOpt)*, 2017.
- [9] Yongguo Mei, Yung-Hsiang Lu, Y. C. Hu, and C. S. G. Lee, "Energy-efficient motion planning for mobile robots," in *IEEE International Conference on Robotics and Automation, Proceedings ICRA '04*, vol. 5, 2004, pp. 4344–4349 Vol.5.
- [10] S. Liu and D. Sun, "Minimizing energy consumption of wheeled mobile robots via optimal motion planning," *IEEE/ASME Transactions on Mechatronics*, vol. 19, no. 2, pp. 401–411, 2014.
- [11] Y. Zhao, Y. Wang, M. Zhou, and J. Wu, "Energy-optimal collision-free motion planning for multi-axis motion systems: An alternating quadratic programming approach," *IEEE Transactions on Automation Science and Engineering*, vol. 16, no. 1, pp. 327–338, 2019.
- [12] T. Setter and M. Egerstedt, "Energy-constrained coordination of multi-robot teams," *IEEE Transactions on Control Systems Technology*, vol. 25, no. 4, pp. 1257–1263, 2017.
- [13] G. Carabin, E. Wehrle, and R. Vidoni, "A review on energy-saving optimization methods for robotic and automatic systems," *Robotics*, vol. 6, no. 4, 2017.
- [14] D. González, J. Pérez, V. Milanés, and F. Nashashibi, "A review of motion planning techniques for automated vehicles," *IEEE Transactions on Intelligent Transportation Systems*, vol. 17, no. 4, pp. 1135–1145, 2016.
- [15] Y. Yan and Y. Mostofi, "Co-optimization of communication and motion planning of a robotic operation under resource constraints and in fading environments," *IEEE Transactions on Wireless Communications*, vol. 12, no. 4, pp. 1562–1572, 2013.
- [16] U. Ali, H. Cai, Y. Mostofi, and Y. Wardi, "Motion-communication co-optimization with cooperative load transfer in mobile robotics: An optimal control perspective," *IEEE Transactions on Control of Network Systems*, vol. 6, no. 2, pp. 621–632, 2019.
- [17] Y. Wu, B. Zhang, S. Yang, X. Yi, and X. Yang, "Energy-efficient joint communication-motion planning for relay-assisted wireless robot surveillance," in *IEEE Conference on Computer Communications (INFOCOM)*, 2017, pp. 1–9.
- [18] C. Tatino, N. Pappas, I. Malanchini, L. Ewe, and D. Yuan, "On the benefits of network-level cooperation in millimeter-wave communications," *IEEE Transactions on Wireless Communications*, vol. 18, no. 9, pp. 4408–4424, 2019.
- [19] Q. Zhang, W. Saad, and M. Bennis, "Millimeter wave communications with an intelligent reflector: Performance optimization and distributional reinforcement learning," *IEEE Transactions on Wireless Communications*, 2021.
- [20] P. Wang, J. Fang, X. Yuan, Z. Chen, and H. Li, "Intelligent reflecting surface-assisted millimeter wave communications: Joint active and passive precoding design," *IEEE Transactions on Vehicular Technology*, vol. 69, no. 12, pp. 14960–14973, 2020.
- [21] E. Basar, M. Di Renzo, J. De Rosny, M. Debbah, M. Alouini, and R. Zhang, "Wireless communications through reconfigurable intelligent surfaces," *IEEE Access*, vol. 7, pp. 116753–116773, 2019.
- [22] C. Liaskos et al., "A new wireless communication paradigm through software-controlled metasurfaces," *IEEE Communications Magazine*, vol. 56, no. 9, pp. 162–169, 2018.
- [23] E. Björnson, Ö. Özdogan, and E. G. Larsson, "Intelligent reflecting surface versus decode-and-forward: How large surfaces are needed to beat relaying?" *IEEE Wireless Communications Letters*, vol. 9, no. 2, pp. 244–248, 2020.
- [24] C. Huang, A. Zappone, G. C. Alexandropoulos, M. Debbah, and C. Yuen, "Reconfigurable intelligent surfaces for energy efficiency in wireless communication," *IEEE Transactions on Wireless Communications*, vol. 18, no. 8, pp. 4157–4170, 2019.
- [25] E. F. Flushing, L. M. Gambardella, and G. A. Di Caro, "Simultaneous task allocation, data routing, and transmission scheduling in mobile multi-robot teams," in *IEEE/RSJ International Conference on Intelligent Robots and Systems (IROS)*, 2017, pp. 1861–1868.
- [26] J. Fink, A. Ribeiro, and V. Kumar, "Robust control of mobility and communications in autonomous robot teams," *IEEE Access*, vol. 1, pp. 290–309, 2013.
- [27] J. Stephan, J. Fink, V. Kumar, and A. Ribeiro, "Concurrent control of mobility and communication in multirobot systems," *IEEE Transactions on Robotics*, vol. 33, no. 5, pp. 1248–1254, 2017.
- [28] S. Gil, S. Kumar, D. Katabi, and D. Rus, "Adaptive communication in multi-robot systems using directionality of signal strength," *The International Journal of Robotics Research*, vol. 34, pp. 946 – 968, 2015.
- [29] J. Sachs, K. Wallstedt, F. Alriksson, and G. Eneroth, "Boosting smart manufacturing with 5G wireless connectivity," *Ericsson Technology Review*, 2019.
- [30] C. Pielli, T. Ropitault, and M. Zorzi, "The potential of mmwaves in smart industry: Manufacturing at 60 GHz," in *17th International Conference on Ad Hoc Networks and Wireless (AD HOC-NOW)*, 2018, pp. 64–76.
- [31] S. Saponara, F. Giannetti, B. Neri, and G. Anastasi, "Exploiting mm-wave communications to boost the performance of industrial wireless networks," *IEEE Transactions on Industrial Informatics*, vol. 13, no. 3, pp. 1460–1470, 2017.
- [32] C. Tatino, N. Pappas, and D. Yuan, "Multi-robot association-path planning in millimeter-wave industrial scenarios," *IEEE Networking Letters*, vol. 2, no. 4, pp. 190–194, 2020.
- [33] L. Zhang et al., "A survey on 5G millimeter wave communications for UAV-assisted wireless networks," *IEEE Access*, vol. 7, pp. 117460–117504, 2019.
- [34] Y. Zeng and R. Zhang, "Energy-efficient UAV communication with trajectory optimization," *IEEE Transactions on Wireless Communications*, vol. 16, no. 6, pp. 3747–3760, 2017.
- [35] A. Alsharafa and M. Yuksel, "Energy efficient D2D communications using multiple UAV relays," *IEEE Transactions on Communications*, vol. 69, no. 8, pp. 5337–5351, 2021.
- [36] E. Fountoulakis, G. S. Paschos, and N. Pappas, "UAV trajectory optimization for time constrained applications," *IEEE Networking Letters*, vol. 2, no. 3, pp. 136–139, 2020.
- [37] M. Hua et al., "Power-efficient communication in UAV-aided wireless sensor networks," *IEEE Communications Letters*, vol. 22, no. 6, pp. 1264–1267, 2018.
- [38] G. Zhang, X. Ou, M. Cui, Q. Wu, S. Ma, and W. Chen, "Cooperative UAV enabled relaying systems: Joint trajectory and transmit power optimization," *IEEE Transactions on Green Communications and Networking*, 2021.
- [39] S. Zhang and R. Zhang, "Radio map-based 3D path planning for cellular-connected UAV," *IEEE Transactions on Wireless Communications*, vol. 20, no. 3, pp. 1975–1989, 2021.
- [40] L. Ge, P. Dong, H. Zhang, J. Wang, and X. You, "Joint beamforming and trajectory optimization for intelligent reflecting surfaces-assisted UAV communications," *IEEE Access*, vol. 8, pp. 78702–78712, 2020.
- [41] S. Li, B. Duo, X. Yuan, Y. Liang, and M. Di Renzo, "Reconfigurable intelligent surface assisted UAV communication: Joint trajectory design and passive beamforming," *IEEE Wireless Communications Letters*, vol. 9, no. 5, pp. 716–720, 2020.
- [42] K. Guo, C. Wang, Z. Li, D. W. K. Ng, and K.-K. Wong, "Multiple UAV-borne 5G-assisted millimeter wave multicast communications: A joint optimization framework," *IEEE Communications Letters*, 2021.
- [43] X. Mu, Y. Liu, L. Guo, J. Lin, and R. Schober, "Intelligent reflecting surface enhanced indoor robot path planning: A radio map based approach," *IEEE Transactions on Wireless Communications*, 2021.
- [44] X. Zhang, A. Liniger, and F. Borrelli, "Optimization-based collision avoidance," *IEEE Transactions on Control Systems Technology*, 2020.
- [45] B. R. Marks and G. P. Wright, "A general inner approximation algorithm for nonconvex mathematical programs," *Operations Research*, vol. 26, no. 4, pp. 681–683, 1978.